inorganics

MDPI

Article

Synthesis and Characterization of Green Zinc-Metal-Pillared Bentonite Mediated Curcumin Extract (Zn@CN/BE) as an Enhanced Antioxidant and Anti-Diabetes Agent

Stefano Bellucci [1,*], Hassan Ahmed Rudayni [2], Marwa H. Shemy [3,4], Malak Aladwani [2], Lina M. Alneghery [2], Ahmed A. Allam [5] and Mostafa R. Abukhadra [4,6,*]

1 INFN-Laboratori Nazionali di Frascati, Via E. Fermi 54, 00044 Frascati, Italy
2 Department of Biology, College of Science, Imam Muhammad bin Saud Islamic University, Riyadh 11623, Saudi Arabia; harudayni@imamu.edu.sa (H.A.R.)
3 Chemistry Department, Faculty of Science, Beni-Suef University, Beni-Suef 65211, Egypt
4 Materials Technologies and Their Applications Lab, Geology Department, Faculty of Science, Beni-Suef University, Beni-Suef 65214, Egypt
5 Zoology Department, Faculty of Science, Beni-Suef University, Beni-Suef 62514, Egypt
6 Geology Department, Faculty of Science, Beni-Suef University, Beni-Suef 65214, Egypt
* Correspondence: stefano.bellucci@lnf.infn.it (S.B.); abukhadra89@science.bsu.edu.eg (M.R.A)

Abstract: Green zinc-metal-pillared bentonite mediated curcumin extract (Zn@CN/BE) was synthesized and characterized as a low-cost and multifunctional (curcumin-based phytochemicals, zinc-capped curcumin, zinc/curcumin complexes, and zinc-pillared bentonite) antioxidant and antidiabetic agent with enhanced activity. The activities of the Zn@CN/BE structure were assessed in comparison with curcumin and ZnO as individual components and in the presence of miglitol and acarbose commercial drugs as controls. The structure validated remarkable antioxidant activities against the common oxidizing radicals (nitric oxide (94.7 ± 1.83%), DPPH (96.4 ± 1.63%), ABTS (92.8 ± 1.33%), and superoxide (62.3 ± 1.63 %)) and inhibition activities against the main oxidizing enzymes (porcine α-amylase (89.3 ± 1.13%), murine α-amylase (70.8 ± 1.54%), pancreatic α-Glucosidase (99.3 ± 1.23%), intestinal α-Glucosidase (97.7 ± 1.24%), and amyloglucosidase (98.4 ± 1.64%)). The reported activities are higher than the activities of individual components and the studied ascorbic acid as well as the commercial drugs. This enhancement effect was assigned to the impact of the zinc pillaring process within the curcumin/bentonite host, which induced the stability, dispersions, and interactive interface of the essential active compounds in addition to the solubility and release rate of the intercalated curcumin extract. This paper recommends the application of the Zn@CN/BE structure as an enhanced, low-cost, biocompatible, safe, and simply produced antioxidant and antidiabetic agent.

Keywords: bentonite; curcumin; zinc metal; pillaring; antioxidant; anti-diabetes

Citation: Bellucci, S.; Rudayni, H.A.; Shemy, M.H.; Aladwani, M.; Alneghery, L.M.; Allam, A.A.; Abukhadra, M.R. Synthesis and Characterization of Green Zinc-Metal-Pillared Bentonite Mediated Curcumin Extract (Zn@CN/BE) as an Enhanced Antioxidant and Anti-Diabetes Agent. *Inorganics* **2023**, *11*, 154. https://doi.org/10.3390/inorganics11040154

Academic Editor: Carlos Martínez-Boubeta

Received: 14 February 2023
Revised: 27 March 2023
Accepted: 30 March 2023
Published: 2 April 2023

1. Introduction

During later periods, humanity will face an eventual increase in the number of diabetes patients in the world. It is predicted that by 2030, diabetes, as clinical pancreatic syndrome, will be the seventh leading cause of death in the world and might affect up to 366 million persons [1–3]. There are two types of diabetes disease: (1) type-1 diabetic mellitus (T1-DM)) and (2) type-2 diabetes mellitus (T2-DM). The latter is the most widely identified type and might affect 90% of the diabetes patients in 2030 [1,4]. T2-DM is a stark type of metabolic disorder and is usually associated with post-prandial hyperglycemia (high concentration of glucose) in addition to the release of free-oxidizing radicals (reactive oxygen species (ROS)) at abnormal levels [5,6]. The T2-DM type of diabetes causes several types of clinical complications such as neuropathy, coronary heart disease, cardiomyopathy, morbidity,

nephropathy, retinopathy, kidney failure, and even mortality [7,8]. Additionally, other types of health side effects are widely reported as a result of high levels of blood sugar, such as polyphagia, polydipsia, and glycosuria [6,9]. Additionally, high levels of ROS cause remarkable pathophysiological conditions that involve the significant fading of the essential antioxidant defenses in the body and result in strong oxidative stress [6,10]. Such oxidative stresses strongly induces lipid peroxidation, insulin resistance, damage to blood vessels, and the destruction of cellular organelles [6,9,11].

However, there are several species of commercially used antidiabetic drugs (biguanides, thiazolidinedione, miglitol, sulfonylureas, acarbose, and voglibose) that achieve significant efficiency during the reduction of hyperglycemia and the oxidizing radicals [6,9,12]. However, their applications are commonly associated with some side effects, such as hepatotoxicity, abdomen distention, meteorism, diarrhea, and severe hypoglycemia [6,13]. Therefore, several types of multifunctional structures have been produced as potential antioxidant and antidiabetic agents that exhibit enhanced management impacts on T2-DM diabetes and prevention properties against oxidative stress [6,14]. Later, different metals and metal oxides-based structures were evaluated as effective antidiabetic materials as a result of their unique physicochemical properties in addition to their significant safety, surface area, biocompatibility, biological activity, and therapeutic and theranostic potentiality [1,14,15]. On the other hand, numerous types of edible plants and their leaves were assessed as safe antioxidant and antidiabetic products, either as raw samples or their extracts [9,14,16]. The valuable phytochemicals of these plants, such as polyphenols, glucosinolates, tannins, terpenes, carotenoids, and steroids, strongly reduce the level of blood sugar as well as the commonly reported complications of T2-DM [7,10,17].

Zinc and its oxide- or hybrid-based structures have been widely investigated as promising bioactive materials that exhibit notable safety, biocompatibility, nontoxicity, and antidiabetic and antioxidant properties [18–20]. Zinc was identified as one of the most vital elements in the organs of the human body that are essential components during the production of protein and nucleic acid [15,19]. Additionally, it is extensively used in several biological and medical applications, including drug delivery and tissue engineering, and as an antioxidant, anticancer, antibacterial, and hypoglycaemic agent [15,21]. However, the studies introduced in this field demonstrate significant effects for crystallinity, morphology, synthesis methods, mechanical stability, crystallite size, hybridization, and surface-modification processes on the biological activities and biomedical applications of zinc-based materials [15,18,22]. Moreover, the assessed zinc-based complexes with different species of biopolymers and the active phytochemicals based on the extracts of plants have resulted in enhanced bioactive products of enhanced biocompatibility, with antioxidant and genotoxicity properties [19,23–25]. Therefore, the green fabrication of zinc-based nanomaterials, utilizing the extracts of edible plants, which are saturated with different species of well-known phytochemicals such as turmeric rhizome, might result in products of enhanced antioxidant and antidiabetic potentiality. This technique was recommended strongly for obtaining non-agglomerated nanoparticles, which are characterized by low production cost, simple fabrication procedures, non-toxicity, and biosafety [18,26]. Moreover, the obtained nanoparticles have been significantly coated with the capping films of the present phytochemicals, such as phenolic compounds, alkaloids, amino acids, and proteins, i.e., the structure presents as a metal/phytochemicals complex [18].

Curcumin (CN) is a polyphenolic natural compound and is extracted from the known turmeric rhizome (Curcuma longa), which exhibits considerable antioxidant, antibacterial, anti-inflammatory, antitumor, and anticancer properties [27,28]. Its low water solubility, poor bioavailability, low chemical stability, and rapid metabolism behavior place strong restrictions on the commercial use of curcumin in different medical applications [28–30]. It was reported that the encapsulation of curcumin or its based extract in effective carriers, or the integration of it into complexes with different metals and metal oxides, can enhance its solubility as well as its biological activity, including its antioxidant and antidiabetic properties [27,31–33]. The application of natural bentonite as a substrate for zinc oxide and

the zinc/curcumin complex, as well as a host for curcumin, will result in an innovative and enhanced multifunctional antioxidant and antidiabetic agent. Bentonite is a widely used natural biocompatible clay mineral that exhibits unique physicochemical properties that could be incorporated extensively into numerous medical and pharmaceutical and medical industries, especially as a drug delivery system [34–36]. Bentonite is characterized by its high natural reserves, ion exchange capacity, surface reactivity, surface area, non-toxicity, biocompatibility, adsorption, and absorption capacity, which validate its value as a carrier for specific metal or drugs as it can enhance physicochemical properties as well as biological activity [34,37].

Therefore, this study aims to synthesize Zn-pillared bentonite mediated curcumin extract (Zn@CN/BE) by the facile intercalation of the organic molecules of the curcumin extract within the bentonite layers, followed by the green pillaring of zinc metal by the same extract, as a safe reducing and capping agent. The synesthetic composite was characterized as an enhanced multifunctional antidiabetic and antioxidant agent with several species of bioactive compounds and chemical groups (curcumin-based phytochemicals, zinc-capped curcumin, zinc/curcumin complexes, and zinc-pillared bentonite). This was performed in comparative and synergetic studies, as compared to pure curcumin, commercial ZnO, green ZnO, bentonite, Zn-pillared bentonite, and curcumin-intercalated bentonite, in addition to the previously tested compounds in the literature.

2. Results and Discussion

2.1. Characterization of the Synthetic Structure

2.1.1. Structural Properties

The structural effects of the integration reaction as well as the crystalline phases were assessed according to the obtained XRD patterns of the final composite as well as the raw materials (Figure 1). The used bentonite precursor demonstrates the characteristic peaks of montmorillonite, the main component of bentonite, in addition to some kaolinite and quartz impurities. The essential montmorillonite diffraction peaks were recognized clearly at 5.78° (001) and 6.95° (002), and other identification peaks were detected at 19.85°, 21.54°, 26.68°, and 28.56° (Ref. card No: 000-003-0010)) (Figure 1A (A)). The montmorillonite phase in the used bentonite sample exhibits 12.9 nm and 12.71 Å as the average crystallite size and basal spacing, respectively. The activation of bentonite with acid resulted in notable structural changes in the montmorillonite crystallinity (Figure 1A (B)). The essential peaks deviated notably to lower 2Theta positions (5.05° and 6.6°) and there was an obvious reduction in the intensities of these peaks, which is in agreement with the previously reported structural effects of acid activation processes on montmorillonite structure (Figure 1A (B)) [38–40]. These features signify the partial destruction impact of the acid activation step on the bentonite crystalline structure, which is commonly associated with the enhancement of textural properties and physicochemical properties, including the surface reactivity and the chemical functional groups.

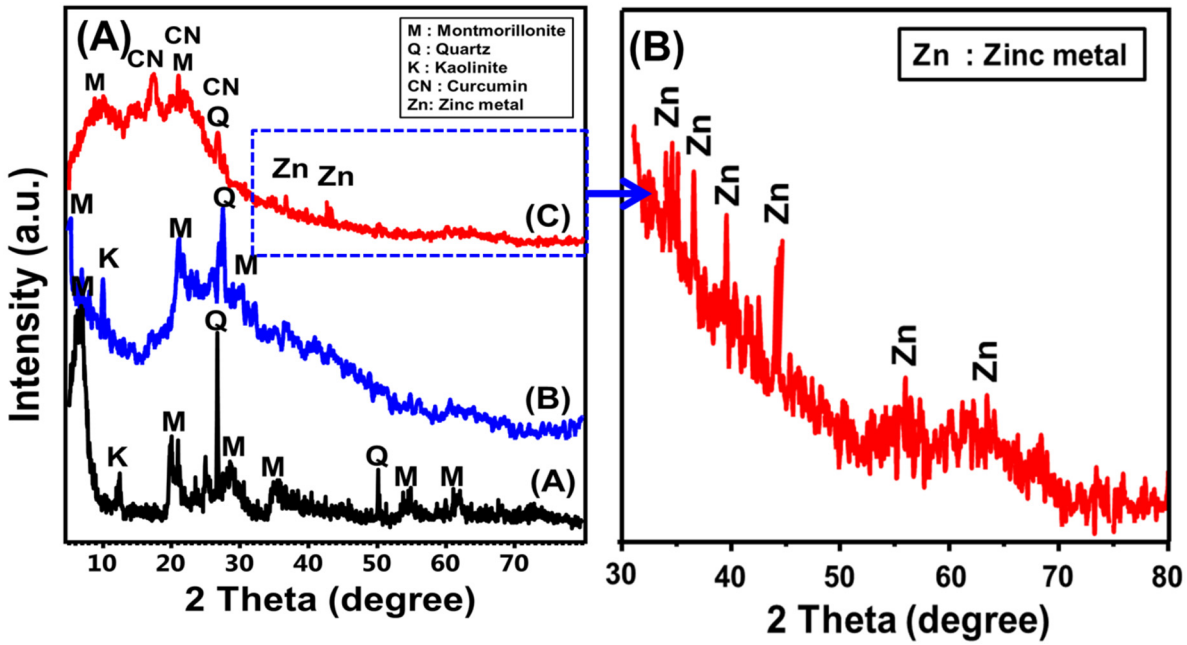

Figure 1. Shows (**A**) XRD patterns of the studied materials (bentonite (**A** (A)), acid-activated bentonite (**A** (B)), and synthetic Zn@CN/BE structure (**A** (C))) and (**B**) focus image on the diffraction patterns of the pillared zinc metal.

The resulting XRD pattern of the formed Zn@CN/BE demonstrates the significant intercalation of the curcumin-based phytochemicals as well as the formation of the pillared metal (Figure 1A (C)). The intercalation of the curcumin organic phytochemicals as well as the successful pillaring of the montmorillonite layers with zinc result in strong exfoliation effects on the structure of the bentonite layers, causing partial destruction for the crystalline structure and partial amorphization, with a notable increase in the basal spacing to 26.3 Å (Figure 1A (C)) [41]. Moreover, there is a notable detection of two identification diffraction peaks of curcumin (12.2°, 14.42°, and 19.5°), which signify its intercalation within the bentonite layers at a significant ratio (Figure 1A (C)). The formation of the pillared metals was confirmed by the detection of much-reduced peaks, which was identified as significant on the high-intensification scale within the area from 30° to 80°. The diffraction peaks characterize the formation of zinc metal with a crystallite size of 10.8 nm, according to the Debye–Scherer formula. The characteristic diffraction peaks were identified at 36.41° (002), 39.08° (100), 43.3° (101), 54.4° (102) and 36.4° (101) (Figure 1A (C),B) (PDF. card: 04-0831; JCPDS 36–1451; JCPDS no. 00-004-0784).

2.1.2. Morphological and Textural Properties

The morphological features were assessed to investigate the impact of the different modification and hybridization steps. This was investigated based on the SEM and the HRTEM images of the different products (Figure 2). The used bentonite host in its SEM images appears as notable aggregated clusters composed of stacked and compacted flakey particles, which normally signify the layered features of the clay minerals (Figure 2A). The characteristic cornflakes structure of montmorillonite structure was clearly detected in the high-magnification SEM images (Figure 2B). The montmorillonite platelets exhibited flexed and curvature properties, which provide the general form of the secondary type of lenticular pores (Figure 2B). Regarding the HRTEM images, the bentonite particles displayed a notable and significant multilayered internal structure with the characteristic lattice figure structure that is widely detected for montmorillonite layered units (Figure 2C).

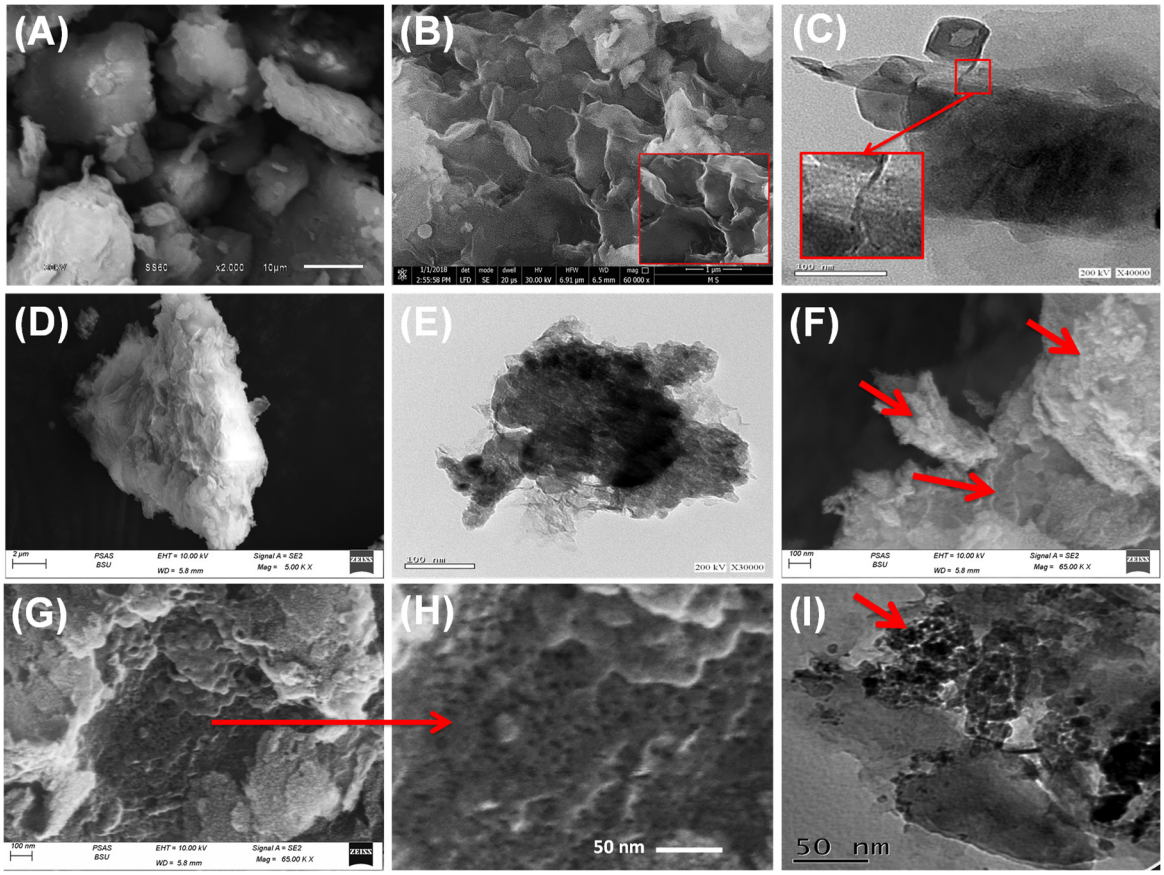

Figure 2. SEM image of raw bentonite (**A**), high-magnification SEM image on the surface of bentonite, and the selected area portrays the cornflakes structure of montmorillonite (**B**), HRTEM images of the used raw bentonite (**C**), SEM image of CN/BE particles, (**D**) HRTEM image of the synthetic CN/BE particles (**E**), SEM image for the surface of the synthetic Zn@CN/BE structure (red arrows refer to the decorated Zn metal on the surface) (**F**), high-magnification image of the supported zinc nanoparticles and the interstitial pores (**G**,**H**), and HRTEM image of the synthetic Zn@CN/BE structure (red arrows refer to the pillared zinc metal between the bentonite layers) (**I**).

After the intercalation process of the bentonite layered units with the extracted curcumin-based organic phytochemicals, the bentonite layers swelled and exfoliated significantly, which appeared during the significant displacement of the layers from each other (Figure 2D). The internal structure, according to the HRTEM images, also reflects the hybridization of the bentonite layers, with the thin films of the polymeric organic compounds that were extracted from the curcumin powder (Figure 2E). They exhibit observable fibrous forms with a dark-grey tone, as compared to the silicate layers of the bentonite host (Figure 2E).

The synthetic Zn@CN/BE structure exhibits a highly decorated exfoliated layer with numerous nanoparticles of the synthetic green zinc metal with spherical shapes (Figure 2F). The growth and distribution of these green zinc nanometals, commonly involved in interstitial nano-pores, significantly positively affected the surface area of the structure (Figure 2G,H). Regarding the HRTEM images of the structure, they support the SEM images significantly. The synthetic zinc-metal nanoparticles were detected between the bentonite layers, which confirms their formation as pillared structures as well as surface-coated layers (Figure 2I).

The morphological effects of the intercalation and pillaring processes resulted in notable textural changes in terms of porosity as well as the surface area of the obtained hybrid structure. The determined surface areas of raw bentonite (BE), acid-activated bentonite (A.BE), curcumin-intercalated bentonite (CN/BE), and the prepared zinc-pillared

bentonite mediated curcumin extract (Zn@CN/BE) are 91 m^2/g, 98.7 m^2/g, 106.3 m^2/g, and 156.7 m^2/g, respectively. The notable enhancement in the surface area after the intercalation process with the curcumin-based organic phytochemicals was assigned to the expansion and swelling impact of these long organic chains on the basal spacing of the layered bentonite units. Additionally, the formation of the zinc metal as pillared nanoparticles between the bentonite layers gives the structure highly porous properties, which also induce the surface area. Moreover, the reported morphological features of the coated zinc layer, as spherical nanoparticles with numerous interstitial nano-pores, on the surface of the exfoliated bentonite sheet also significantly enhanced the surface area.

2.1.3. Chemical Properties

The synthesis procedures and the impact of the hybridization processes were based on the FT-IR spectra of the raw samples as well as the synthetic products (Figure 3). The incorporated bentonite precursor exhibited the characteristic spectrum of the montmorillonite chemical structure, demonstrating its essential functional groups such as the coordination of –OH (3400 cm^{-1}) with the octahedral cations (Al_2OH, AlMg(OH) and $AlFe^{3+}$(OH)) and the interlayer water molecules between the montmorillonite layers (1640 cm^{-1}) (Figure 3 (A)). The structural Si-O as well as Al-O chemical groups were recognized based on the reported bands of around 1000 cm^{-1} and 918 cm^{-1}, respectively. The signified bands within the estimation range from 1000 cm^{-1} to 400 cm^{-1} identify the structural bonds of Si–O–Al, Si-O-Si, Si–O–Mg, and Mg–Fe–OH (Figure 3 (A)) [42,43]. The detected spectrum of the acid-activated bentonite exhibits no significant detection for new bands or the removal of the original bands (Figure 3 (B)). The structural effect of the process was signified by the notably deviated absorption bands in addition to the observable increase in the intensity of the characteristic bands of the interlayer water molecules, as well as the coordinated hydroxyl groups within the phyllosilicate structure of montmorillonite, which occurred as a result of the hydration properties of the performed acid treatment step (Figure 3 (B)). Moreover, the previous results are in agreement with the XRD studies that signify the non-extensive destruction properties of the acid-modification process on the crystalline structure of the montmorillonite units (Figure 3 (B)).

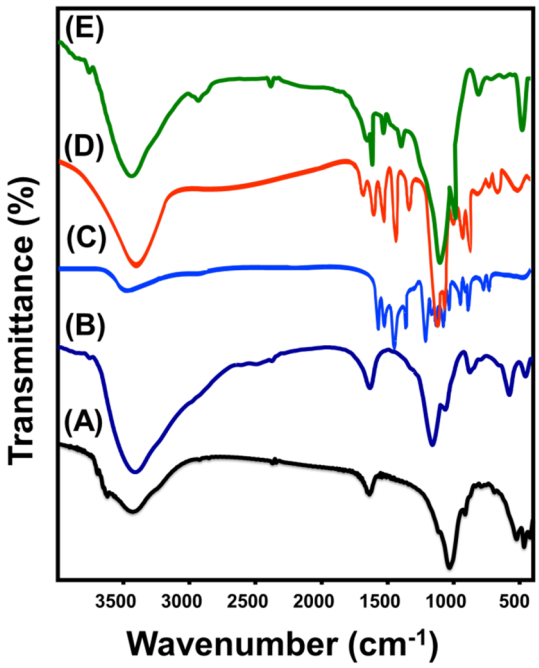

Figure 3. FT–IR spectrum of raw bentonite (A), acid-activated bentonite (B), curcumin powder (C), synthetic CN/BE composite (D), and synthetic Zn@CN/BE composite (E).

The obtained spectrum of the used curcumin powder exhibits the commonly identified bands of its main chemical groups, including the –OH groups of the present organic phenolic compounds (3506 cm^{-1}), aromatic -C-H groups of the neat curcumin (2943–2965 cm^{-1}), C=C bonds (1626 cm^{-1}), the structural benzene ring of curcumin (1604 cm^{-1}), vibration stretching of C=O bonds (1507 cm^{-1}), C-H bond of olefin groups (1432 cm^{-1}), C-O bonds of the aromatic groups (1278 cm^{-1}), C-H bonds of the aromatic groups (1162 and 812 cm^{-1}), the vibration of C-O-C groups (1023 cm^{-1}); benzoatetrans-CH (963 cm^{-1}), and the cis-CH of the aromatic structure (716 cm^{-1}) (Figure 3 (C)) [28,35,44]. The spectrum of the synthetic curcumin-intercalated bentonite sheets (CN/BE) was compared with the spectra of the integrated raw materials of bentonite and curcumin (Figure 3 (D)). The identified bands demonstrate the successful combination of the inorganic structure of bentonite and the organic chemical groups of the curcumin-based extract (Figure 3 (D)). The interaction between them was signified by the remarkable shifting in the positions of the identification bands of the essential chemical groups, as compared to the original samples (Figure 3 (D). The marked inorganic functional groups of bentonite layers are Si-O-Si (473.2 cm^{-1}), Si–O–Al (534 cm^{-1}), Al-O (934 cm^{-1}), and Si-O (1008 cm^{-1}), while the marked organic functional groups of the curcumin extract are benzoatetrans-CH (921 cm^{-1}), aromatic C-O (1284 cm^{-1}), olefin C-H (1440 cm^{-1}), C=O (1509 cm^{-1}), and benzene rings (1612 cm^{-1}) (Figure 3 (D)).

Such changes in the functional chemical groups were also identified in the determined FT-IR spectrum of the synthetic Zn@CN/BE hybrid structure (Figure 3 (E)). The organic chemical groups of the curcumin-based phytochemicals as well as the inorganic aluminosilicate chemical groups of bentonite were clearly identified, with a considerable deviation of the bands demonstrating the impact of the zinc pillaring processes (Figure 3 (E)). Moreover, the reduced absorption bands of around 602.7 cm^{-1} and 462 cm^{-1} signify the Zn-O bonds and the entrapping of the metal (Figure 3 (E)) [24,26]. This is in notable agreement with the obtained results from the dispersive X-ray spectrum (EDX) of the composite (Figure S1). The elemental composition based on the EDX spectrum demonstrates the existence of Si and Al as inorganic elements related to the bentonite host, the C element signifies the organic component of the composite (curcumin extract), and the Zn element signifies the pillared and coated zinc nanoparticles.

2.2. Antioxidant Properties

2.2.1. Scavenging of Nitric Oxide

The aerobic respiration and electron transportation processes resulted in several species of ROS that normally cause significant oxidative stress and several types of degenerative diseases [45]. Nitric oxide, which is a common gaseous free reactive oxygen radical, can cause numerous hazardous side effects [6,46]. The abnormal levels of nitric oxide cause the fragmentation of DNA, death of neuronal cells, cell cytotoxicity, and damage to the cells [47]. The metal and metal oxide-based structures were categorized as potential antioxidant materials that can be applied effectively against the nitric oxide radicals (Figure 4A). The experimentally detected scavenging percentage of nitric oxide radicals by the synthetic Zn@CN/BE multifunctional structure is 94.7 ± 1.83% (Figure 4A). This value is higher than the determined values of pure curcumin extract (CN) (12.3 ± 1.06%), bentonite-intercalated curcumin CN/BE (23.6 ± 1.17%), commercial ZnO nanoparticles (35.7% ± 1.57 %), and green synthesized ZnO (48.7 ± 1.36%), as well as the commonly used commercial ascorbic acid as the control sample (21.6 ± 1.33%) (Figure 4A). These results validate the significant effect of the used bentonite host on the achieving efficiency of the curcumin as well as the zinc. This effect might be assigned to the impact of the clay host in enhancing the dispersion properties, stability, exposure, and interactive interface area between the loaded biologic active compound (Zn and curcumin-based phytochemicals) and the nitric oxide radicals, which in turn enhance their capture [48,49]. Moreover, the encapsulation of curcumin within the bentonite host induces the biological and solubility properties of curcumin in addition to the reported significant adsorption and absorption

capacity of the bentonite structure [42,50]. Therefore, the synthetic green zinc-pillared bentonite mediated curcumin extract (Zn@CN/BE) was recommended as a multifunctional organic/inorganic antioxidant structure of significant scavenging efficiency for the active free nitric oxide radical.

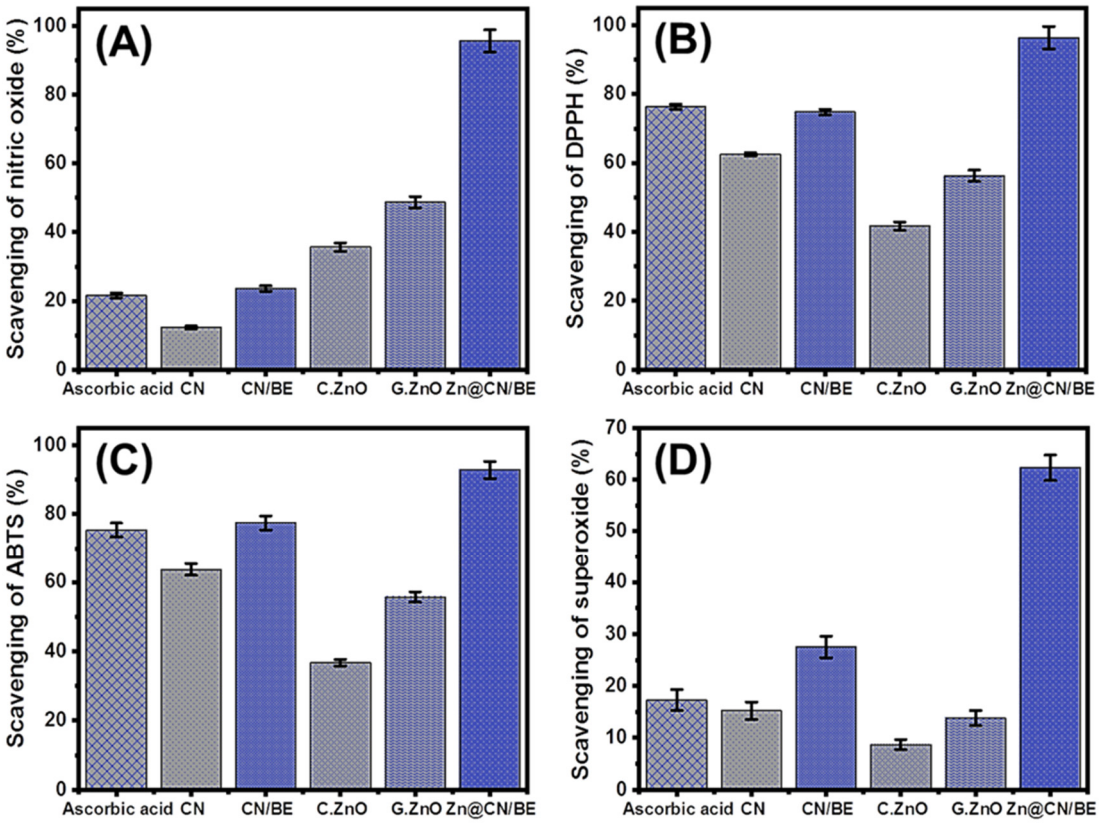

Figure 4. The antioxidant activities of CN, CN/BE, commercial ZnO, green ZnO, and Zn@CN/BE structures (100 µg/mL) (the tests were replicated 5 times); (**A**) Nitric oxide scavenging activities (20 µL; 100 µg/mL); (**B**) DPPH scavenging activities (20 µL; 100 µg/mL); (**C**) ABTS scavenging activities (10 µL; 100 µg/mL); and (**D**) superoxide radical scavenging activities (100 µL; 100 µg/mL).

2.2.2. Scavenging of DPPH Radical

The scavenging properties of the prepared Zn@CN/BE composite against the DPPH oxidation radicals were estimated in comparison with CN, CN/BE commercial ZnO, green ZnO, and ascorbic acid as the commonly used control or standard. The estimated scavenging percentage of DPPH by the Zn@CN/BE composite is 96.4 ± 1.63%, which is a significantly high value considering the obtained value by the control (ascorbic acid (76.3 ± 1.28%)) as well as the determined values using commercial ZnO (41.7± 1.58%), green ZnO (56.3 ± 1.37%), CN extract (62.5 ± 1.62%) and CN-intercalated bentonite (CN/BE) (74.8 ± 1.41%) (Figure 4B). Moreover, the determined activity is notably higher than several tested compounds in the literature, such as CuO (about 80%) [51], Ag-doped ZnO (73.79%) [6], RGO-ZnO NCs (69%) [4], Ag nanoparticles (67%) [52], Pt nanoparticles (70%) [53], and Au nanoparticles (70.73%) [54]. The DPPH scavenging mechanisms by the metal-based antioxidant agents such as Zn@CN/BE composite occurred by the effective transfer process of an electron (e^-) and a proton (H^+) from its structure to the organic structure of the DPPH radical [55]. This is commonly known as the coupled proton/electron transfer mechanism, where electron density can be transmitted from the surface of the pillared zinc metal to the odd electrons within the nitrogen atoms of the DPPH structure [35]. Hosting the zinc metal as a biologically active and antioxidant structure between the bentonite layers significantly enhances the efficiency of the previous mechanisms. The saturation of the bentonite layers with numerous negative charges induces

the charge separation efficiencies involving electron attraction reactions, causing a notable enhancement in the scavenging properties of Zn@CN/BE, considering the previously reported mechanism [55,56].

2.2.3. Scavenging of ABTS Radical

The scavenging of ABTS was later introduced as a significant indictor of the antioxidant properties of different synthetic materials, especially hybrid structures or composites, depending on the generated reduction in the ABTS cation radical ($ABTS^{\bullet+}$), which is commonly produced using potassium persulfate. It was reported that the synthetic structures that characterize hydrogen-donating antioxidant behaviors can be applied defectively to reduce the level of the released $ABTS^{\bullet+}$ radical in the cells. Therefore, the prepared Zn@CN/BE structure with its essential components (pillared zinc metal and curcumin-based phytochemicals) is a highly effective antioxidant agent against the $ABTS^{\bullet+}$ radical. The capturing percentage of the ABTS radical by the Zn@CN/BE composite is 92.8 ± 1.33%, which is a significantly promising value when considering the value obtained by the control (ascorbic acid (75.4 ± 1.14%)) as well as the values determined using commercial ZnO (36.4 ± 1.45%), green ZnO (55.7 ± 1.44%), CN extract (63.7 ± 1.35%) and CN-intercalated bentonite (CN/BE) (77.4 ± 1.83%) (Figure 4C). Additionally, the reported activity of the composite is higher than the compounds investigated in the literature, such as oregano oil/halloysite [57], soy β-conglycinin-dextran-polyphenol [50], mung bean protein [58], and chitosan/lignosulfonate micelles [59]. The results obtained during these synergetic tests demonstrate the enhancement properties of the composite as compared to the main components, which were assigned previously associated with an enhancement in the quantities of the active chemical groups as well as the textural and physicochemical properties. Moreover, the expected wrapping of the intercalated curcumin-based long-chain organic phytochemicals between the aluminosilicate layers of bentonite strongly induces the generation of numerous hydrogen atoms [48].

2.2.4. Scavenging of Superoxide Radical

The superoxide anion radical ($O_2^{\bullet-}$) is a common oxidizing radical that generates widely in cellular organelles involving mitochondria. This radical is commonly immediately transformed into active species of hydroxyl radicals (•OH) in addition to hydrogen peroxide (H_2O_2). The generation of reactive hydroxyl radicals and the non-regulation of its concentrations in the cells commonly cause severe pathophysiological conditions and associated degenerative diseases in addition to several types of hazardous health risks [60]. Superoxide radicals and their transformed species exhibit strong cellular damage effects, especially on DNA, RNA, and protein [61]. However, the system of the human body provides a natural defense against the generated superoxide radicals to maintain safe physiological homeostasis, but in various diseases, the organs cannot provide the suitable functional groups or the required levels of these functional groups to overcome the concentrations of the released superoxide radical. Therefore, the scavenging of superoxide radicals by innovative and biocompatible synthetic structures is strongly recommended (Figure 4D). The measured scavenging percentage of $O_2^{\bullet-}$ using Zn@CN/BE (62.3 ± 1.63%) is an excellent value as compared to the reported structure in the literature and the used standard (ascorbic acid (17.3 ± 1.34%)) (Figure 4D). Additionally, the synergetic tests demonstrate the significant enhancement effects of the different steps of the integration process on the antioxidant properties of the structure gains of the superoxide radical. The determined values using commercial ZnO, green ZnO, CN extract, and CN/BE are 8.7 ± 1.16%, 13.8 ± 1.22%, 15.2 ± 1.66%, and 27.5 ± 1.31%, respectively (Figure 4D). Moreover, the activity of Zn@CN/BE is significantly higher than that of the previously addressed structures in the literature, such as Ag-doped ZnO (27.34%) [6], Ag nanoparticles [52], and CuO (about 80%) [51]. This qualifies the prepared Zn@CN/BE as a green multifunctional antioxidant product to be used effectively against generated $O_2^{\bullet-}$ radicals in the human cells.

2.3. Antidiabetic Properties

2.3.1. Porcine Pancreatic α-Amylase Inhibition Assay

The antidiabetic properties of the zinc-pillared bentonite mediated curcumin extract (Zn@CN/BE) were evaluated against several enzymes, including α-amylase enzymes, which are categorized as a highly effective and dominant species of digestive enzymes. They exhibit strong destruction and breakdown effects on the long chains of carbohydrate polymeric structures, such as polysaccharide starch-producing maltose simple structures, which in turn transform immediately into glucose [6]. Therefore, the effective inhibition of α-amylase enzymes will significantly reduce the breakdown rate of the complex sugar compounds and in turn the absorption rate of dietary starches and the actual levels of the blood sugar [62]. Therefore, post-prandial hyperglycemia in diabetes can be controlled at significant and safe levels [24]. The determined inhibition % of the α-amylase enzyme (porcine pancreatic) using Zn@CN/BE (89.3 ± 1.13%) reflects its significant antidiabetic properties, considering the values determined by the commercially used drugs as standards (acarbose (75.2 ± 1.68%) and miglitol (18.3 ± 1.42%)) (Figure 5A). Moreover, the detailed synergetic studies display an enhancement in the inhibition percentage of curcumin extract (CN) after its intercalation within the aluminosilicate layers of bentonite (CN/BE), and the inhibition efficiency of the composite (CN/BE) was strongly enhanced after the pillaring of the structure with green zinc metal nanoparticles. The measured inhibition % of α-amylase using commercial ZnO, green ZnO, CN extract, and CN/BE are 40.3 ± 1.66%, 44.5 ± 1.53%, 54.3 ± 1.46%, and 60.7 ± 1.77%, respectively (Figure 5A). Additionally, the determined activity of Zn@CN/BE is notably higher than Ag-doped ZnO (23%) [6], RGO-ZnO (51.19%) [4], Ag/CuO (38.9%) [63], NiO nanoparticles (22%) [64], Ag nanoparticle (61%) [52], and the synthetic Fe-CuO-SiO_2 composite [65], which are structures studied in the literature.

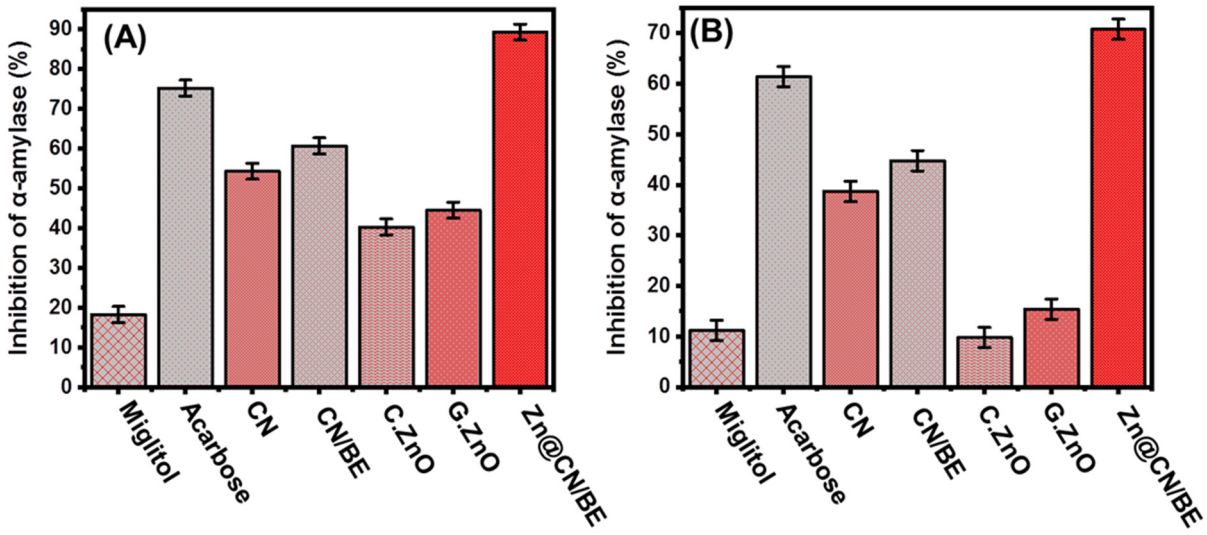

Figure 5. The α-amylase inhibition activities of CN, CN/BE, commercial ZnO, green ZnO, and Zn@CN/BE structures (500 µL; 100 µg/mL) (the tests were replicated 5 times); (**A**) Porcine pancreatic α-amylase enzyme (100 µL; 50 µg/mL); and (**B**) Murine pancreatic α-amylase enzyme (100 µL; 50 µg/mL).

This enhancement effect might be related to the impact of the bentonite host or carrier on controlling the diffused rates on the intercalated curcumin-based biologically active phytochemicals, which maintain the interaction between these compounds and the enzyme for significant intervals [42]. Moreover, the significant surface area of the applied bentonite carrier induces the stability and dispersion properties of the loaded active compounds (pillared zinc and curcumin phytochemicals). Additionally, the presence of the loaded zinc nanoparticles in the pillared and non-agglomerated forms between the bentonite

layers enhances their exposure and interaction interfaces with the enzyme. Previous studies demonstrated the significant adverse effects of the agglomeration processes on the biological activities of the synthetic metal and metal oxide nanoparticles [48]. The obtained enhancement effect of the applied host on the biological and antidiabetic activities of the organic and metal-based active compounds are in agreement with the reported results in the literature [14,28,48,60]. Based on the determined inhibition efficiency of Zn@CN/BE against the porcine pancreatic α-amylase enzymes, it can be applied effectively as an enhanced and safe antidiabetic agent, considering the commonly detected side effects of the commercially applied drugs as well as their expensive costs [66,67].

2.3.2. Murine Pancreatic α-Amylase Inhibition

The inhibition properties of Zn@CN/BE against the murine pancreatic α-amylase were assessed to signify the qualification of the composite to be used against the commercially studied enzymes as well as the metabolically crude active enzymes. The tests were conducted in synergetic systems, considering the effect of the different combinations and hybridization procedures. The application of Zn@CN/BE caused an inhibition of the α-amylase enzyme (murine pancreatic) of 70.8 ± 1.54%, demonstrating higher activity than the common antidiabetic drugs used as controls (acarbose (61.4 ± 1.55%) and miglitol (11.2 ± 1.61%)) (Figure 5B). The synergetic tests also demonstrated the significant impact of the hybridization process on inducing the antidiabetic activity of the essential active compounds of curcumin and the pillared zinc-metal nanoparticles. The measured inhibition % using commercial ZnO, green ZnO, CN extract, and CN/BE were 9.8 ± 1.12%, 15.4 ± 1.11%, 38.7 ± 1.33%, and 44.8 ± 1.52%, respectively (Figure 5B). Therefore, the prepared Zn@CN/BE composite exhibits an enhanced inhibition effect on the α-amylase enzyme, either the commercial type (porcine pancreatic) or the metabolically crude active enzyme (murine pancreatic), as compared to the commercial drug or the individual components of curcumin and zinc oxide.

2.3.3. Pancreatic α-Glucosidase Inhibition

The inhibition properties of Zn@CN/BE against the α-Glucosidase enzymes were assessed as they are the most vital enzymes during the essential metabolic reactions of the dietary carbohydrates. Therefore, the significant inhibition of these enzymes with a suitable agent will strongly reduce the absorption rate and efficiency of the glucose in the blood and will be associated with significant suppression effects on hyperglycemia [18]. The inhibition effect of the synthetic Zn@CN/BE on the pancreatic α-Glucosidase enzymes is close to 100%, achieving significant activity as compared to the commercial controls of the antidiabetic drugs (miglitol and acarbose) and several investigated zinc and zinc oxide-based synthetic antidiabetic structures (Figure 6A). The estimated inhibition effects of CN (75.6 ± 1.37%), CN/BE (83.5 ± 1.48%), commercial ZnO (68.7 ± 1.44%), and green ZnO (77.3 ± 1.27%) (Figure 6A) are in agreement with the previously obtained inhibition effects on the α-amylase enzymes. Additionally, they show the significant enhancement impact of the hybridization process and the bentonite carrier on the biological activities of the loaded active compounds by enhancing the stability, curcumin release rate, and exposure interface of zinc. Moreover, the synthesis of the pillared zinc-metal nanoparticles based on the curcumin extract might result in a curcumin/zinc complex structure or zinc capped with thin forms of the curcumin-based phytochemicals, especially the biophenol-compounds, which exhibit higher inhibition properties than the synthesized pillared clay by transitional chemical methods [18]. The determined activity of Zn@CN/BE is notably higher than Ag-doped ZnO (91.19%) [6], Ag/CuO (19.6%) [63], and RGO-ZnO (53.24%) [4] as studied materials in the literature.

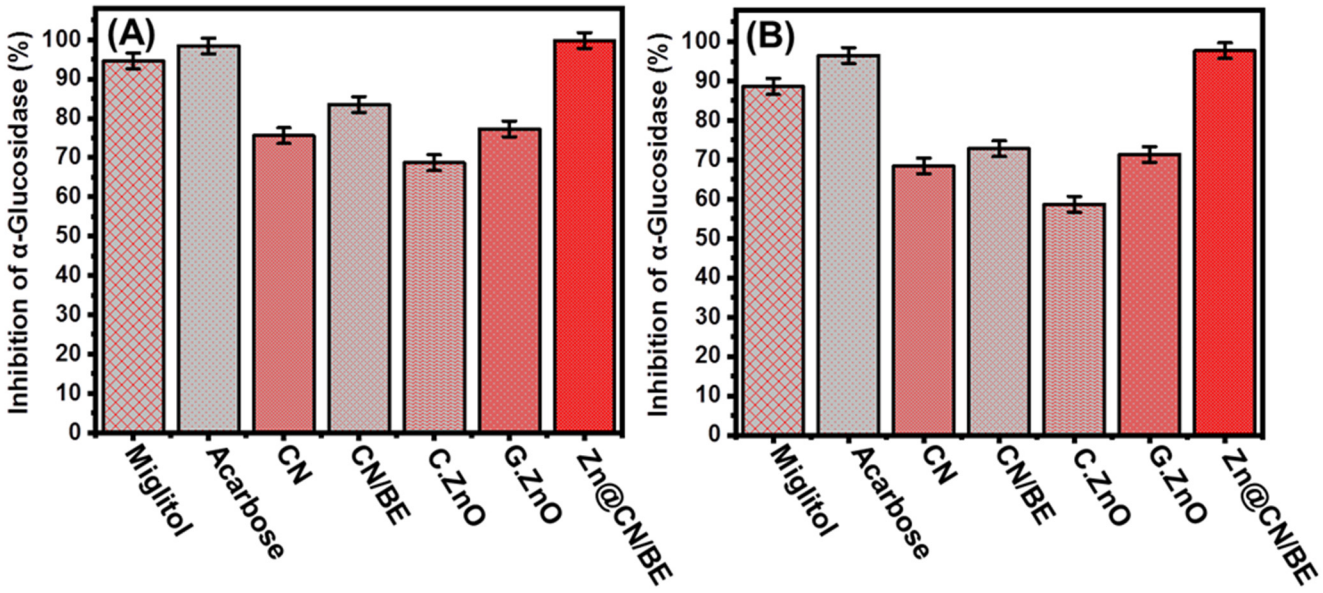

Figure 6. The α-Glucosidase inhibition activities of CN, CN/BE, commercial ZnO, green ZnO, and Zn@CN/BE structures (200 µL; 100 µg/mL) (the tests were replicated 5 times); (**A**) Pancreatic α-Glucosidase enzyme (100 µL; 0.1 unit/mL); and (**B**) Murine intestinal α-Glucosidase enzyme (100 µL; 0.1 unit/mL).

2.3.4. Murine Intestinal α-Glucosidase Inhibition

In addition to the commercial pancreatic α-Glucosidase enzymes, the inhibition properties of the prepared Zn@CN/BE composite were tested against crude active murine intestinal glucosidase enzymes. The results also demonstrate the significant inhibition effects of the synthetic composite on the crude active glucosidase enzymes, with an experimental percentage of 97.7 ± 1.24%, which is notably higher than the results determined by the commercial antidiabetic drugs such as miglitol and acarbose (Figure 7B). Additionally, the synergetic results portray the enhanced biological activity and the inhibition effects of Zn@CN/BE on the murine intestinal α-Glucosidase enzymes, as compared to CN extract (68.4 ± 1.27%), CN/BE (72.8 ± 1.51%), commercial ZnO (58.7 ± 1.46%), and green synthesized ZnO (71.3 ± 1.16%) (Figure 6B). Several studies demonstrate the significant antidiabetic properties of the zinc-based structures, which can strongly reduce the actual levels of glucose in the blood in addition to having a significant enhancement effect on the serum insulin, glucokinase activity, insulin receptor, and glucokinase genes [68].

2.3.5. Amyloglucosidase Inhibition

The amyloglucosidase enzymes also exhibit strong effects on the breakdown of the starch and the absorption rates of the dietary starches. Therefore, the inhibition of this type of enzyme will also have significant reduction effects on the efficiency of the conversion of the present complex sugar compound into simple species [69]. The inhibition properties of the Zn@CN/BE composite against the amyloglucosidase enzymes were assessed in synergetic studies and compared to the integrated components. The Zn@CN/BE structure exhibits a strong inhibition effect on the enzyme, achieving an inhibition percentage of 98.4 ± 1.64%, which is a promising value as compared to the determined value using commercial drugs at the same conditions (miglitol (88.3 ± 1.83%) and acarbose (95.6 ± 1.72%)) (Figure 7). Additionally, this value is notably higher than the measured inhibition percentages using CN extract (65.8 ± 1.35%), CN/BE (83.4 ± 1.47%), commercial ZnO (65.4 ± 1.27%), and green synthesized ZnO (70.5 ± 1.77%) (Figure 7). Therefore, the prepared green zinc-pillared bentonite mediated curcumin extract (Zn@CN/BE) in this study represents a promising antidiabetic agent of notable high biocompatibility and low

production cost, with few side effects and strong inhibition effects on the essential enzymes responsible for diabetic mellitus diseases.

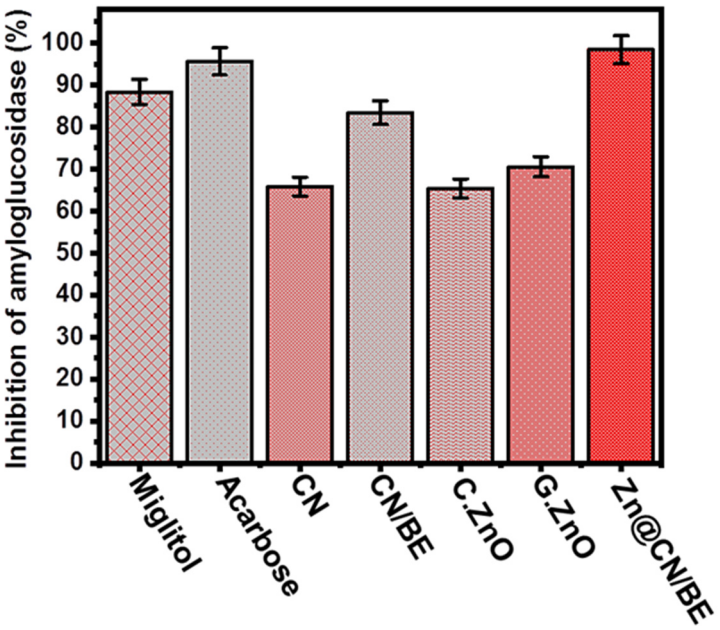

Figure 7. The amyloglucosidase (100 µL; 0.1 unit/mL) inhibition activities of CN, CN/BE, commercial ZnO, green ZnO, and Zn@CN/BE structures (100 µL; 100 µg/mL) (the tests were replicated 5 times).

3. Experimental Work

3.1. Materials and Chemicals

Natural bentonite (54.82% (SiO_2), 2.6% (Na_2O), 17.56% (Al_2O_3), 2.5% (MgO), 9.5% (Fe_2O_3), 2.4% (CaO), 1.45% (TiO_2), and 9.2% (LOI)) was obtained from a bentonite quarry in the Western Desert, Egypt. Sulfuric acid (99%), curcumin (>94.99%), absolute ethanol, hydrazine solution (35 wt %), and zinc nitrate hexahydrate (98%) were obtained from Sigma-Aldrich, Egypt, and were applied during the synthesis procedures of the composite. Moreover, α-amylase, para-nitrophenyl α-glucopyranoside (pNPG), 1,1-diphenyl-2-picrylhydrazil (DPPH), α-Glucosidase, L-ascorbic acid, starch, phosphate buffer, and 2,2′-azino-bis(3-ethylbenzothiazoline-6-sulphonic acid (ABTS) were delivered from Sigma-Aldrich, Egypt, and used during the antioxidant and antidiabetic tests.

3.2. Synthesis of Green Zinc-Pillared Bentonite Mediated Curcumin Extract (Zn@CN/BE)

3.2.1. Acid Activation of Bentonite

The activation of the bentonite structure with acid was carried out to dispose of the present metallic and carbonate impurities. Thus, 10 g of bentonite powder was dispersed within the diluted sulfuric acid solution (20%; 100 mL) and the homogenization between them was conducted by a magnetic stirrer (650 rpm) for 12 h at 100 °C. After that, the acid-activated bentonite powder was extracted by filtration using Whatman filter paper. The filtrated products were washed thoroughly and neutralized with distilled water, dried under room conditions for 48 h (40.3 °C), and kept in specific containers for further synthesis steps.

3.2.2. Synthesis of Curcumin-Intercalated Bentonite (CN/BE)

The intercalation of the bentonite layers with the phytochemicals of curcumin was performed using a facile organic intercalation technique. Firstly, the curcumin extract was prepared by the dispersion of the curcumin powder (3.7 g) within ethanol (100 mL; 60%) for about 15 min in a closed system at 50 °C, and the mixture was homogenized by stirring (1500 rpm). After this step, the mixture was treated by sonication waves (20 min;

240 W) to induce the homogenization degree and the extraction efficiency of the essential phytochemicals. Then, 50 mL of the resulting curcumin-based extract was mixed homogenously with previously prepared bentonite colloid solution (4.4 g of bentonite + 50 mL of distilled water). The obtained mixture was kept under very fast stirring (1500 rpm) for 12 h and sonicated for an additional 5 h (240 W), to induce the intercalation efficiency of the dissolved phytochemicals of curcumin within the layered structure of bentonite. After that, the intercalated solid particles were filtrated from the intercalation solutions, washed thoroughly for five runs (10 min), and dried gently at 50 °C for 12 h to be used in the next step (Figure 1).

3.2.3. Synthesis of Zinc-Pillared Bentonite Mediated Curcumin Extract (Zn@CN/BE)

The synthesis procedures started with the production of the curcumin-based extract as the essential green reagent, which was used as a reducing and capping agent. On the other side, the bentonite/$Zn(NO_3)_2{\cdot}6H_2O$) mixture was prepared by the homogenization of the intercalated bentonite fractions (4.4 g) within the aqueous solution of zinc nitrate (2.2 g; 100 mL). The homogenization between the two components was continued for 10 h using a magnetic stirrer (650 rpm) and then by a sonication source (240 W) for an additional 2 h. After that, the curcumin-based extract (100 mL) was mixed with the bentonite/$Zn(NO_3)_2{\cdot}6H_2O$) mixture under continuous high-speed stirring (1500 rpm) until the observable detection of a dark-red precipitate. This was followed by the sudden addition of a hydrazine solution of 50 mL to confirm the successful conversion of early formed oxides or hydroxides into metallic Zn (II). The reaction continued for an additional 24 h under stirring, including five intervals of sonication treatment (20 min) to ensure effective homogenization between the different reactants and to maintain the homogenous distribution of the pillared ions or the adsorbed phytochemicals. After that, the Zn-pillared curcumin-intercalated bentonite, as solid particles (Zn@CN/BE), was separated effectively by filtration using Whitman filter paper. The filtrated product was washed for five runs with distilled water, with each washing run continuing for 10 min, and the washed product was dried for 12 h at 50 °C (Figure 8).

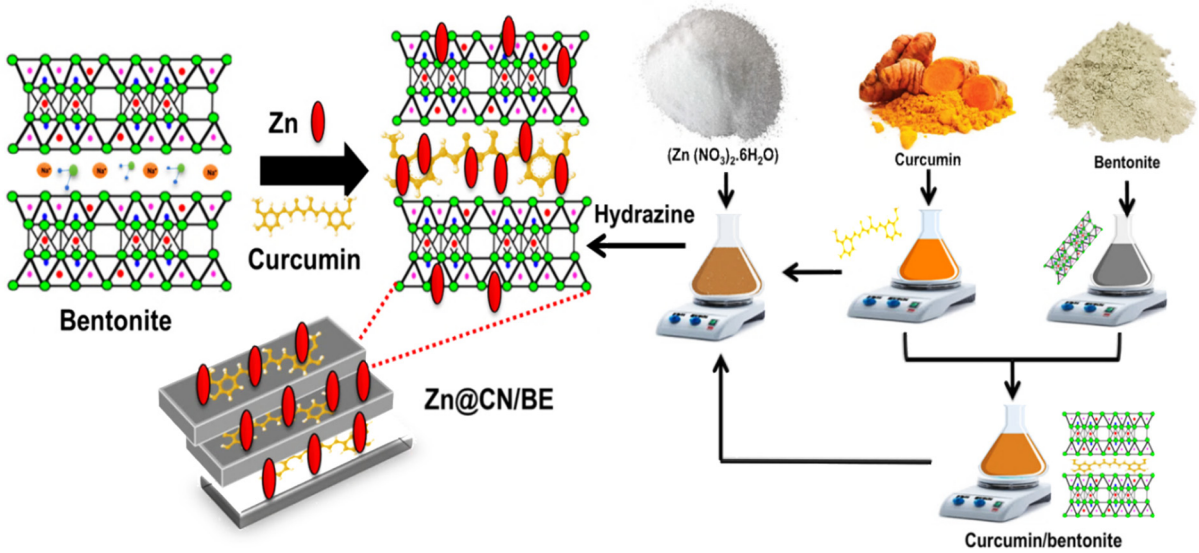

Figure 8. Schematic diagram for the synthesis procedures of the Zn@CN/BE composite.

3.3. Characterization Techniques

The crystallinity and the structural impacts of the performed modification and integration processes were illustrated based on the X-ray diffraction patterns of the resulting products using a PANalytical-Empyrean X-ray diffractometer with a determination range from 5 to 80°. The impact of the modification reactions and the successful incorporation of the active chemical groups were monitored based on the FT-IR spectra of the products

obtained by a Fourier Transform Infrared spectrometer (FTIR−8400S; Shimadzu) within the frequency range of 400 cm^{-1} to 4000 cm^{-1}. The changes in the external morphology as well as the internal properties were investigated using a Scanning Electron Microscope (Gemini, Zeiss-Ultra 55) and a Transmission Electron Microscope (JEOL-JEM2100), respectively. The impact of the integration reactions on the textural properties and the surface area was assessed using a surface area analyzer (Beckman Coulter SA3100), considering the resulting N_2 adsorption/desorption isotherm curves.

3.4. Antioxidant Studies

3.4.1. Nitric Oxide Radical Scavenging Assay

This was inspected based on the reported procedures by Kitture et al. [70]. The evaluated structures (20 µL; 100 µg/mL) were mixed effectively with sodium nitroprusside (2 mL; 10 mM) in previously prepared saline phosphate buffer (500 µL; pH 7.4), and this mixture was incubated at 25 °C for 150 min. Then, about 500 µL of this mixture was extracted and homogenized with 1 mL of diluted sulphanilic acid (33% sulphanilic acid+ 20% glacial acetic acid). The obtained mixture after this stage was incubated again for an additional 5 min, and this was followed by the careful addition of naphthyl ethylenediamine dihydrochloride (0.1% *w*/*v*; 1 mL) before an additional re-incubation stage for an additional 30 min. The absorbance was detected using a microplate reader at 540 nm, and the differences between the reported values of the control samples and the existence of the structures were used to determine the scavenging percentage according to Equation (1).

$$Scavenging\ (\%) = \frac{A540_{Control} - A540_{Test}}{A540_{Control}} \times 100 \quad (1)$$

3.4.2. DPPH Radical Scavenging Assay

The scavenging tests of DPPH were conducted according to the methodology reported by Robkhob et al. [6]. The prepared materials (20 µL; 100 µg/mL)) were homogenized with prepared methanolic solution (80 µL) containing 2, 2-diphenyl-1-picrylhydrazyl (DPPH, 100 µM) in specific 96-well plates. After this step, the obtained homogenous mixture was incubated for about 20 min in the dark. The absorbance was detected using a microplate reader at 517 nm, and the differences between the reported values of the control samples and in the existence of the structures were used to determine the scavenging percentage according to Equation (2).

$$Scavenging\ (\%) = \frac{A517_{Control} - A517_{Test}}{A517_{Control}} \times 100 \quad (2)$$

3.4.3. ABTS Radical Scavenging Assay

This test was executed according to the technique mentioned by Dappula et al. [71]. ABTS stock solution (7 mm) was firstly prepared by the direct dissolving of ABTS (44 mg) in deionized water (10 mL). This solution was mixed effectively within potassium persulfate solution (3 µL) to produce the free cations of ABTS radicals ($ABTS^{\bullet+}$), after a reaction interval in the dark for 18 h at 25 °C. After the generation of $ABTS^{\bullet+}$, the system was diluted with methanol at an adjusted ratio of 1:29 to obtain freshly mit $ABTS^{\bullet+}$. Then, the materials (10 µL; 100 µg/mL) were mixed with the ABTS solution (290 µL) for 30 min. The absorbance was detected using a microplate reader at 734 nm, and the differences between the reported values of the control samples and in the existence of the structures were used to determine the scavenging percentage according to Equation (3).

$$Scavenging\ (\%) = \frac{A734_{Control} - A734_{Test}}{A734_{Control}} \times 100 \quad (3)$$

3.4.4. Superoxide Radical Scavenging Assay

This assay was conducted according to the experimental steps reported by Robkhob et al. [6]. The prepared materials (100 µL; 100 µg/mL) were mixed separately with EDTA solutions (200 µL; 12 mM), riboflavin solutions (100 µL; 20 µg), NBT (100 µL; 0.1 mg), and ethanol (200 µL) mixture. Afterward, this mixture was diluted using phosphate buffer (50 mM; 3 mL) and exposed for 5 min to an illumination source. The absorbance was detected using a microplate reader at 540 nm, and the differences between the reported values of the control samples and in the existence of the structures were used to determine the scavenging percentage according to Equation (4).

$$Scavenging\ (\%) = \frac{A540_{Control} - A540_{Test}}{A540_{Control}} \times 100 \quad (4)$$

3.5. Antidiabetic Studies

3.5.1. Porcine Pancreatic Amylase Inhibition Assay

This type of assay, which used the evaluated materials, was carried out as a commonly investigated antidiabetic indicator based on Robkhob et al. [6]. The synthetic materials at certain dosages (500 µL; 100 µg/mL) were incubated with the tested porcine pancreatic α-amylase enzyme (100 µL; 50 µg/mL) at 37 °C for 10 min. This incubation step was followed by the incorporation of starch as a substrate (1 %). After that, the absorbance of α-amylase was detected using a microplate reader at 540 nm, and the differences between the reported values of the control samples and in the existence of the structures were used to determine the scavenging percentage according to Equation (5).

$$Inhibition\ (\%) = \frac{A540_{Control} - A540_{Test}}{A540_{Control}} \times 100 \quad (5)$$

3.5.2. Crude Murine Pancreatic Amylase Inhibition Assay

This assay was performed to assess the inhibition impact of the synthetic materials on the commercial enzymes as well as the crude enzyme to ensure the antidiabetic properties of these materials. The pancreas of a Swiss male mouse (10 weeks old) was used as the source of crude enzyme. The pancreas was firstly incorporated into the starvation step for 12 h and then excised and dispersed within a specific saline phosphate buffer, which was supplemented carefully with the protease inhibitors. After that, the cell-free supernatant was extracted from the system using centrifugation processes for 15 min at an adjusted speed of 10,000 rpm; it was diluted to achieve an absorbance of 0.4 at 280 nm; and it was used as the source of the crude enzyme. The assay tests of the crude murine pancreatic amylase enzyme were conducted as previously reported in Section 3.5.2.

3.5.3. α-Glucosidase Inhibition Assay

This type of inhibition assay, on α-Glucosidase using the evaluated materials, was carried out according to Sanap et al. [72]. The prepared materials (200 µL; 100 µg/mL) were mixed homogenously with the α-Glucosidase enzyme (100 µL; 0.1 unit/mL) and the mixture was incubated at 37 °C for 60 min. After that, 10 mL of the pNPG was mixed with the incubated system and re-incubated for an additional 10 min. By the end of the incubation interval, the reaction was stopped using a prepared solution of Na_2CO_3 (2 mL; 0.1 M). Finally, the absorbance of the released nitrophenol molecules from the used pNPG was measured by a microplate reader at 420 nm, and the measured values were used to determine the inhibition percentages according to Equation (6).

$$Inhibition\ (\%) = \frac{A420_{Control} - A420_{Test}}{A420_{Control}} \times 100 \quad (6)$$

3.5.4. Crude Murine Intestinal α-Glucosidase Inhibition Assay

The crude intestinal α-Glucosidase enzyme was obtained using the pancreas of Swiss male mice according to the previously reported experimental procedures considered in Section 3.5.2. After that, the inhibition assay tests of the prepared materials in the presence of crude murine intestinal α-Glucosidase were conducted according to the previously mentioned procedures in Section 3.5.3, but in the presence of substrate of p-nitrophenyl-α-D-glucopyranoside.

3.5.5. Amyloglucosidase Inhibition Assay

The inhibition tests of amyloglucosidase using the prepared materials were based on the experimental procedures presented by Lawande et al. [73]. The assessed materials (100 µL; 100 µg/mL) were mixed homogeneously with the amyloglucosidase enzyme (100 µL; 0.1 unit/mL) and then the mixture was incubated for 10 min at 37 °C in the presence of starch as a substrate (1%). After that, the absorbance of amyloglucosidase was detected using a microplate reader at 540 nm, and the differences between the reported values of the control samples and in the existence of the structures were used to determine the scavenging percentage according to Equation (5).

3.6. Statistical Analysis

All the results were incorporated as their mean values ± the obtained standard errors of the mean values (S.E.M.) and with n equal to 3. The significance properties of the statistical assessment of the results were obtained according to the analysis of variance (ANOVA) results and the paired tests, considering the values of * $p < 0.05$.

4. Conclusions

Green zinc metal-pillared bentonite mediated curcumin extract (Zn@CN/BE) was prepared successfully and characterized as an enhanced low-cost antioxidant and an antidiabetic agent with multifunctional properties (curcumin-based phytochemicals, zinc-capped curcumin, Zn-pillared bentonite, and zinc/curcumin complexes). Zn@CN/BE validates strong antioxidant and antidiabetic activities against common oxidative radicals (nitric oxide (94.7 ± 1.83%), DPPH (96.4 ± 1.63%), ABTS (92.8 ± 1.33%), superoxides (62.3 ± 1.63%)), essential oxidizing enzymes (porcine α-amylase (89.3 ± 1.13%), murine α-amylase (70.8 ± 1.54%), pancreatic α-Glucosidase (99.3 ± 1.23%), intestinal α-Glucosidase (97.7 ± 1.24%), and amyloglucosidase (98.4 ± 1.64%)). These results are significantly higher than the results of the drugs tested as controls (miglitol and acarbose), as well as those of the individual components of the composites (curcumin and ZnO). The obtained results portray the significant enhancement effect of the bentonite carrier on the physiochemical and biological activities of pillared Zn metal and intercalated curcumin-based phytochemicals. Therefore, the synthetic green Zn@CN/BE composite can be recommended as an enhanced, low-cost, biocompatible, safe, and simply produced antioxidant and antidiabetic agent, as compared to commercially used drugs, which will be covered by future in vivo studies.

Supplementary Materials: The following supporting information can be downloaded at: https://www.mdpi.com/article/10.3390/inorganics11040154/s1, Figure S1: EDX spectrum of the synthetic composite.

Author Contributions: Conceptualization, M.R.A., S.B. and H.A.R..; methodology, M.H.S., M.R.A. and H.A.R.; Software, M.H.S., A.A.A. and L.M.A.; validation, M.R.A., S.B., H.A.R., A.A.A. and M.A.; formal analysis, M.H.S., A.A.A., M.A., L.M.A. and L.M.A.; investigation, M.R.A., S.B., H.A.R. and A.A.A.; resources, A.A.A., M.H.S., L.M.A. and L.M.A.; data curation, M.R.A., M.H.S., M.A., L.M.A. and L.M.A.; writing—original draft preparation, M.R.A., M.H.S., M.A., A.A.A., S.B., H.A.R., L.M.A. and L.M.A.; writing—review and editing, M.R.A., H.A.R., M.H.S., A.A.A., S.B., L.M.A. and L.M.A.; visualization, M.R.A., H.A.R. and S.B.; supervision, M.R.A., S.B., A.A.A. and H.A.R.; project administration, M.R.A., H.A.R. and A.A.A.; funding acquisition, S.B. and H.A.R. All authors have read and agreed to the published version of the manuscript.

Funding: This research was funded by [Deanship of Scientific Research at Imam Mohammad Ibn Saud Islamic University (IMSIU)] grant number [RP-21-09-89].

Data Availability Statement: Data are available upon reasonable, by the Corresponding Authors.

Acknowledgments: The authors extend their appreciation to the Deanship of Scientific Research at Imam Mohammad Ibn Saud Islamic University (IMSIU) for funding and supporting this work through the Research Partnership Program no. (RP-21-09-89).

Conflicts of Interest: The authors declare no conflict of interest.

References

1. Arvanag, F.M.; Bayrami, A.; Habibi-Yangjeh, A.; Pouran, S.R. A comprehensive study on antidiabetic and antibacterial activities of ZnO nanoparticles biosynthesized using Silybum marianum L seed extract. *Mater. Sci. Eng. C* **2018**, *97*, 397–405. [CrossRef]
2. Behl, T.; Kaur, I.; Sehgal, A.; Sharma, E.; Kumar, A.; Grover, M.; Bungau, S. Unfolding Nrf2 in diabetes mellitus. *Mol. Biol. Rep.* **2021**, *48*, 927–939. [CrossRef] [PubMed]
3. Billacura, M.P.; Lavilla, C.J.; Cripps, M.J.; Hanna, K.; Sale, C.; Turner, M.D. β-alanine scavenging of free radicals protects mitochondrial function and enhances both insulin secretion and glucose uptake in cells under metabolic stress. *Adv. Redox Res.* **2022**, *6*, 100050. [CrossRef]
4. Hsu, W.-H.; Chang, H.-M.; Lee, Y.-L.; Prasannan, A.; Hu, C.-C.; Wang, J.-S.; Lai, J.-Y.; Yang, J.M.; Jebaranjitham, N.; Tsai, H.-C. Biodegradable polymer-nanoclay composites as intestinal sleeve implants installed in digestive tract for obesity and type 2 diabetes treatment. *Mater. Sci. Eng. C* **2020**, *110*, 110676. [CrossRef]
5. Sagandira, C.R.; Khasipo, A.Z.; Sagandira, M.B.; Watts, P. An overview of the synthetic routes to essential oral anti-diabetes drugs. *Tetrahedron* **2021**, *96*, 132378. [CrossRef]
6. Robkhob, P.; Ghosh, S.; Bellare, J.; Jamdade, D.; Tang, I.-M.; Thongmee, S. Effect of silver doping on antidiabetic and antioxidant potential of ZnO nanorods. *J. Trace Elements Med. Biol.* **2020**, *58*, 126448. [CrossRef] [PubMed]
7. Paul, S.; Hajra, D. Study of glucose uptake enhancing potential of fenugreek (Trigonella foenum graecum) leaves extract on 3T3 L1 cells line and evaluation of its antioxidant potential. *Pharmacogn. Res.* **2018**, *10*, 347. [CrossRef]
8. Feldman, E.L.; Callaghan, B.C.; Pop-Busui, R.; Zochodne, D.W.; Wright, D.E.; Bennett, D.L.; Bril, V.; Russell, J.W.; Viswanathan, V. Diabetic neuropathy. *Nat. Rev. Dis. Prim.* **2019**, *5*, 41. [CrossRef] [PubMed]
9. Dedvisitsakul, P.; Watla-Iad, K. Antioxidant activity and antidiabetic activities of Northern Thai indigenous edible plant extracts and their phytochemical constituents. *Heliyon* **2022**, *8*, e10740. [CrossRef]
10. Kim, M.-S.; Jung, Y.S.; Jang, D.; Cho, C.H.; Lee, S.-H.; Han, N.S.; Kim, D.-O. Antioxidant capacity of 12 major soybean isoflavones and their bioavailability under simulated digestion and in human intestinal Caco-2 cells. *Food Chem.* **2022**, *374*, 131493. [CrossRef]
11. Asmat, U.; Abad, K.; Ismail, K. Diabetes mellitus and oxidative stress—A concise review. *Saudi Pharm. J.* **2016**, *24*, 547–553. [CrossRef] [PubMed]
12. Ben Ahmed, Z.; Hefied, F.; Yousfi, M.; Demeyer, K.; Heyden, Y.V. Study of the antioxidant activity of Pistacia atlantica Desf. Gall extracts and evaluation of the responsible compounds. *Biochem. Syst. Ecol.* **2022**, *100*, 104358. [CrossRef]
13. Yilmazer-Musa, M.; Griffith, A.M.; Michels, A.J.; Schneider, E.; Frei, B. Grape Seed and Tea Extracts and Catechin 3-Gallates Are Potent Inhibitors of α-Amylase and α-Glucosidase Activity. *J. Agric. Food Chem.* **2012**, *60*, 8924–8929. [CrossRef] [PubMed]
14. Malik, A.R.; Sharif, S.; Shaheen, F.; Khalid, M.; Iqbal, Y.; Faisal, A.; Aziz, M.H.; Atif, M.; Ahmad, S.; Fakhar-e-Alam, M.; et al. Green synthesis of RGO-ZnO mediated Ocimum basilicum leaves extract nanocomposite for antioxidant, antibacterial, antidiabetic and photocatalytic activity. *J. Saudi Chem. Soc.* **2022**, *26*, 101438. [CrossRef]
15. Singh, T.A.; Sharma, A.; Tejwan, N.; Ghosh, N.; Das, J.; Sil, P.C. A state of the art review on the synthesis, antibacterial, antioxidant, antidiabetic and tissue regeneration activities of zinc oxide nanoparticles. *Adv. Colloid Interface Sci.* **2021**, *295*, 102495. [CrossRef]
16. Madan, H.R.; Sharma, S.C.; Suresh, D.; Vidya, Y.S.; Nagabhushana, H.; Rajanaik, H.; Anantharaju, K.S.; Prashantha, S.C.; Maiya, P.S. Facile green fabrication of nanostructure ZnO plates, bullets, flower, prismatic tip, closed pine cone: Their antibacterial, antioxidant, photoluminescent and photocatalytic properties. *Spectrochim. Acta Part A Mol. Biomol. Spectrosc.* **2016**, *152*, 404–416. [CrossRef]
17. Ağagündüz, D.; Yılmaz, B.; Koçak, T.; Başar, H.B.A.; Rocha, J.M.; Özoğul, F. Novel Candidate Microorganisms for Fermentation Technology: From Potential Benefits to Safety Issues. *Foods* **2022**, *11*, 3074. [CrossRef]
18. Velsankar, K.; Venkatesan, A.; Muthumari, P.; Suganya, S.; Mohandoss, S.; Sudhahar, S. Green inspired synthesis of ZnO nanoparticles and its characterizations with biofilm, antioxidant, anti-inflammatory, and anti-diabetic activities. *J. Mol. Struct.* **2022**, *1255*, 132420.
19. Ansari, A.; Ali, A.; Khan, N.; Umar, M.S.; Owais, M. Shamsuzzaman Synthesis of steroidal dihydropyrazole derivatives using green ZnO NPs and evaluation of their anticancer and antioxidant activity. *Steroids* **2022**, *188*, 109113. [CrossRef]
20. Noohpisheh, Z.; Amiri, H.; Farhadi, S.; Mohammadi-Gholami, A. Green synthesis of Ag-ZnO nanocomposites using Trigonella foenum-graecum leaf extract and their antibacterial, antifungal, antioxidant and photocatalytic properties. *Spectrochim. Acta Part A Mol. Biomol. Spectrosc.* **2020**, *240*, 118595. [CrossRef]

21. Sharma, A.; Nagraik, R.; Sharma, S.; Sharma, G.; Pandey, S.; Azizov, S.; Chauhan, P.K.; Kumar, D. Green synthesis of ZnO nanoparticles using Ficus palmata: Antioxidant, antibacterial and antidiabetic studies. *Results Chem.* **2022**, *4*, 100509. [CrossRef]
22. Yusof, N.A.A.; Zain, N.M.; Pauzi, N. Synthesis of ZnO nanoparticles with chitosan as stabilizing agent and their antibacterial properties against Gram-positive and Gram-negative bacteria. *Int. J. Biol. Macromol.* **2019**, *124*, 1132–1136. [CrossRef]
23. Shaaban, S.; Adam, M.S.S.; El-Metwaly, N.M. Novel organoselenium-based N-mealanilic acid and its zinc (II) chelate: Catalytic, anticancer, antimicrobial, antioxidant, and computational assessments. *J. Mol. Liq.* **2022**, *363*, 119907. [CrossRef]
24. Meer, B.; Andleeb, A.; Iqbal, J.; Ashraf, H.; Meer, K.; Ali, J.S.; Drouet, S.; Anjum, S.; Mehmood, A.; Khan, T.; et al. Bio-Assisted Synthesis and Characterization of Zinc Oxide Nanoparticles from Lepidium Sativum and Their Potent Antioxidant, Antibacterial and Anticancer Activities. *Biomolecules* **2022**, *12*, 855. [CrossRef] [PubMed]
25. Hasanzadeh, A.; Gholipour, B.; Rostamnia, S.; Eftekhari, A.; Tanomand, A.; Khaksar, S.; Khalilov, R. Biosynthesis of AgNPs onto the urea-based periodic mesoporous organosilica (AgxNPs/Ur-PMO) for antibacterial and cell viability assay. *J. Colloid Interface Sci.* **2021**, *585*, 676–683. [CrossRef] [PubMed]
26. Baran, A.; Keskin, C.; Baran, M.F.; Huseynova, I.; Khalilov, R.; Eftekhari, A.; Irtegun-Kandemir, S.; Kavak, D.E. Ecofriendly Synthesis of Silver Nanoparticles Using Ananas comosus Fruit Peels: Anticancer and Antimicrobial Activities. *Bioinorg. Chem. Appl.* **2021**, *2021*, 2058149. [CrossRef]
27. Prasad, S.; Lall, R. Zinc-curcumin based complexes in health and diseases: An approach in chemopreventive and therapeutic improvement. *J. Trace Elements Med. Biol.* **2022**, *73*, 127023. [CrossRef]
28. Deng, J.; Wang, J.; Hu, H.; Hong, J.; Yang, L.; Zhou, H.; Xu, D. Application of mesoporous calcium silicate nanoparticles as a potential SD carrier to improve the solubility of curcumin. *J. Dispers. Sci. Technol.* **2022**, 1–9. [CrossRef]
29. Kour, P.; Afzal, S.; Gani, A.; Zargar, M.I.; Tak, U.N.; Rashid, S.; Dar, A.A. Effect of nanoemulsion-loaded hybrid biopolymeric hydrogel beads on the release kinetics, antioxidant potential and antibacterial activity of encapsulated curcumin. *Food Chem.* **2022**, *376*, 131925. [CrossRef]
30. Yixuan, L.; Qaria, M.A.; Sivasamy, S.; Jianzhong, S.; Daochen, Z. Curcumin production and bioavailability: A comprehensive review of curcumin extraction, synthesis, biotransformation and delivery systems. *Ind. Crop. Prod.* **2021**, *172*, 114050. [CrossRef]
31. Khansili, N.; Krishna, P.M. Curcumin functionalized TiO2 modified bentonite clay nanostructure for colorimetric Aflatoxin B1 detection in peanut and corn. *Sens. Bio Sens. Res.* **2022**, *35*, 100480. [CrossRef]
32. Roy, S.; Rhim, J.-W. Preparation of carbohydrate-based functional composite films incorporated with curcumin. *Food Hydrocoll.* **2020**, *98*, 105302. [CrossRef]
33. Bernardo, A.; Plumitallo, C.; De Nuccio, C.; Visentin, S.; Minghetti, L. Curcumin promotes oligodendrocyte differentiation and their protection against TNF-α through the activation of the nuclear receptor PPAR-γ. *Sci. Rep.* **2021**, *11*, 1–13. [CrossRef] [PubMed]
34. Abukhadra, M.R.; Adlii, A.; El-Sherbeeny, A.M.; Soliman, A.T.A.; Elgawad, A.E.E.A. Promoting the decontamination of different types of water pollutants (Cd2+, safranin dye, and phosphate) using a novel structure of exfoliated bentonite admixed with cellulose nanofiber. *J. Environ. Manag.* **2020**, *273*, 111130. [CrossRef]
35. Wasim, M.; Shi, F.; Liu, J.; Zhang, H.; Zhu, K.; Tian, Z. Synthesis and characterization of curcumin/MMT-clay-treated bacterial cellulose as an antistatic and ultraviolet-resistive bioscaffold. *J. Polym. Res.* **2022**, *29*, 423. [CrossRef]
36. Mohammadhosseini, S.; Al-Musawi, T.J.; Romero Parra, R.M.; Qutob, M.; Gatea, M.A.; Ganji, F.; Balarak, D. UV and Visible Light Induced Photodegradation of Reactive Red 198 Dye and Textile Factory Wastewater on Fe2O3/Bentonite/TiO2 Nanocomposite. *Minerals* **2022**, *12*, 1417. [CrossRef]
37. Tong, L.; Liang, T.; Tian, Y.; Zhang, Q.; Pan, Y. Research progress on treatment of mine wastewater by bentonite composite. *Arab. J. Geosci.* **2022**, *15*, 681. [CrossRef]
38. Koksal, E.; Afsin, B.; Tabak, A.; Caglar, B. Butylamine-resadiye bentonite composite characterization. *Spectrosc. Lett.* **2020**, *53*, 745–750. [CrossRef]
39. Darmawan, M.A.; Muhammad, B.Z.; Harahap, A.F.P.; Ramadhan, M.Y.A.; Sahlan, M.; Haryuni; Supriyadi, T.; Abd-Aziz, S.; Gozan, M. Reduction of the acidity and peroxide numbers of tengkawang butter (Shorea stenoptera) using thermal and acid activated bentonites. *Heliyon* **2020**, *6*, e05742. [CrossRef]
40. Nagahashi, E.; Ogata, F.; Saenjum, C.; Nakamura, T.; Kawasaki, N. Preparation and Characterization of Acid-Activated Bentonite with Binary Acid Solution and Its Use in Decreasing Electrical Conductivity of Tap Water. *Minerals* **2021**, *11*, 815. [CrossRef]
41. Chauhan, M.; Saini, V.K.; Suthar, S. Ti-pillared montmorillonite clay for adsorptive removal of amoxicillin, imipramine, diclofenac-sodium, and paracetamol from water. *J. Hazard. Mater.* **2020**, *399*, 122832. [CrossRef] [PubMed]
42. Dardir, F.M.; Mohamed, A.S.; Abukhadra, M.R.; Ahmed, E.A.; Soliman, M.F. Cosmetic and pharmaceutical qualifications of Egyptian bentonite and its suitability as drug carrier for Praziquantel drug. *Eur. J. Pharm. Sci.* **2018**, *115*, 320–329. [CrossRef] [PubMed]
43. Abdel Salam, M.; Mokhtar, M.; Albukhari, S.M.; Baamer, D.F.; Palmisano, L.; Jaremko, M.; Abukhadra, M.R. Synthesis and Characterization of Green ZnO@ polynaniline/Bentonite Tripartite Structure (G. Zn@ PN/BE) as Adsorbent for As (V) Ions: Integration, Steric, and Energetic Properties. *Polymers* **2022**, *14*, 2329. [CrossRef] [PubMed]
44. Khatun, B.; Banik, N.; Hussain, A.; Ramteke, A.; Maji, T. Genipin crosslinked curcumin loaded chitosan/montmorillonite K-10 (MMT) nanoparticles for controlled drug delivery applications. *J. Microencapsul.* **2018**, *35*, 439–453. [CrossRef] [PubMed]

45. Dhall, A.; Self, W. Cerium Oxide Nanoparticles: A Brief Review of Their Synthesis Methods and Biomedical Applications. *Antioxidants* **2018**, *7*, 97. [CrossRef] [PubMed]
46. Sharpe, E.; Andreescu, D.; Andreescu, S. Artificial Nanoparticle Antioxidants. In *Oxidative Stress: Diagnostics, Prevention, and Therapy*; American Chemical Society: Washington, DC, USA, 2011; pp. 235–253. [CrossRef]
47. Parul, R.; Kundu, S.K.; Saha, P. In vitro nitric oxide scavenging activity of methanol extracts of three Bangladeshi medicinal plants. *Pharma Innov.* **2013**, *1*, 83.
48. Song, Y.; Yang, F.; Ma, M.; Kang, Y.; Hui, A.; Quan, Z.; Wang, A. Green synthesized Se–ZnO/attapulgite nanocomposites using Aloe vera leaf extract: Characterization, antibacterial and antioxidant activities. *LWT* **2022**, *165*, 113762. [CrossRef]
49. Saad, A.M.; Abukhadra, M.R.; Ahmed, S.A.-K.; Elzanaty, A.M.; Mady, A.H.; Betiha, M.A.; Shim, J.-J.; Rabie, A.M. Photocatalytic degradation of malachite green dye using chitosan supported ZnO and Ce–ZnO nano-flowers under visible light. *J. Environ. Manag.* **2020**, *258*, 110043. [CrossRef]
50. Wang, Z.-J.; Xu, J.-J.; Ji, F.-Y.; Luo, S.-Z.; Li, X.-J.; Mu, D.-D.; Jiang, S.-T.; Zheng, Z. Fabrication and characterization of soy β-conglycinin-dextran-polyphenol nanocomplexes: Improvement on the antioxidant activity and sustained-release property of curcumin. *Food Chem.* **2022**, *395*, 133562. [CrossRef]
51. Ayodhya, D.; Veerabhadram, G. Facile thermal fabrication of CuO nanoparticles from Cu (II)-Schiff base complexes and its catalytic reduction of 4-nitrophenol, antioxidant, and antimicrobial studies. *Chem. Data Collect.* **2019**, *23*, 100259. [CrossRef]
52. Sudha, A.; Jeyakanthan, J.; Srinivasan, P. Green synthesis of silver nanoparticles using Lippia nodiflora aerial extract and evaluation of their antioxidant, antibacterial and cytotoxic effects. *Resour. Technol.* **2017**, *3*, 506–515. [CrossRef]
53. Ramachandiran, D.; Elangovan, M.; Rajesh, K. Structural, optical, biological and photocatalytic activities of platinum nanoparticles using salixtetrasperma leaf extract via hydrothermal and ultrasonic methods. *Optik* **2021**, *244*, 167494. [CrossRef]
54. Hosny, M.; Fawzy, M.; El-Badry, Y.A.; Hussein, E.E.; Eltaweil, A.S. Plant-assisted synthesis of gold nanoparticles for photocatalytic, anticancer, and antioxidant applications. *J. Saudi Chem. Soc.* **2022**, *26*, 101419. [CrossRef]
55. Adersh, A.; Kulkarni, A.R.; Ghosh, S.; More, P.; Chopade, B.A.; Gandhi, M.N. Surface defect rich ZnO quantum dots as antioxidant inhibitingα-amylase and α-glucosidase: A potential anti-diabetic nanomedicine. *J. Mater. Chem. B* **2015**, *3*, 4597–4606.
56. Liu, Y.; Ying, D.; Cai, Y.; Le, X. Improved antioxidant activity and physicochemical properties of curcumin by adding ovalbumin and its structural characterization. *Food Hydrocoll.* **2017**, *72*, 304–311. [CrossRef]
57. Oun, A.A.; Bae, A.Y.; Shin, G.H.; Park, M.-K.; Kim, J.T. Comparative study of oregano essential oil encapsulated in halloysite nanotubes and diatomaceous earth as antimicrobial and antioxidant composites. *Appl. Clay Sci.* **2022**, *224*, 106522. [CrossRef]
58. Mohammadian, M.; Salami, M.; Moghadam, M.; Amirsalehi, A.; Emam-Djomeh, Z. Mung bean protein as a promising biopolymeric vehicle for loading of curcumin: Structural characterization, antioxidant properties, and in vitro release kinetics. *J. Drug Deliv. Sci. Technol.* **2021**, *61*, 102148. [CrossRef]
59. Lin, D.; Xiao, L.; Qin, W.; Loy, D.A.; Wu, Z.; Chen, H.; Zhang, Q. Preparation, characterization and antioxidant properties of curcumin encapsulated chitosan/lignosulfonate micelles. *Carbohydr. Polym.* **2022**, *281*, 119080. [CrossRef]
60. Hamasaki, T.; Kashiwagi, T.; Imada, T.; Nakamichi, N.; Aramaki, S.; Toh, K.; Morisawa, S.; Shimakoshi, H.; Hisaeda, Y.; Shirahata, S. Kinetic Analysis of Superoxide Anion Radical-Scavenging and Hydroxyl Radical-Scavenging Activities of Platinum Nanoparticles. *Langmuir* **2008**, *24*, 7354–7364. [CrossRef]
61. Xie, J.; Wang, N.; Dong, X.; Wang, C.; Du, Z.; Mei, L.; Yong, Y.; Huang, C.; Li, Y.; Gu, Z.; et al. Graphdiyne Nanoparticles with High Free Radical Scavenging Activity for Radiation Protection. *ACS Appl. Mater. Interfaces* **2018**, *11*, 2579–2590. [CrossRef]
62. Shu, G.; Xu, D.; Xie, S.; Chang, L.-J.; Liu, X.; Yang, J.; Li, Y.; Wang, X. The antioxidant, antibacterial, and infected wound healing effects of ZnO quantum dots-chitosan biocomposite. *Appl. Surf. Sci.* **2023**, *611*, 155727. [CrossRef]
63. Selvan, D.S.A.; Kumar, R.S.; Murugesan, S.; Shobana, S.; Rahiman, A.K. Antidiabetic activity of phytosynthesized Ag/CuO nanocomposites using Murraya koenigii and Zingiber officinale extracts. *J. Drug Deliv. Sci. Technol.* **2022**, *67*, 102838. [CrossRef]
64. Haritha, V.; Gowri, S.; Janarthanan, B.; Faiyazuddin; Karthikeyan, C.; Sharmila, S. Biogenic synthesis of nickel oxide nanoparticles using Averrhoa bilimbi and investigation of its antibacterial, antidiabetic and cytotoxic properties. *Inorg. Chem. Commun.* **2022**, *144*, 109930. [CrossRef]
65. Sabeena, G.; Rajaduraipandian, S.; Manju, T.; Alhadlaq, H.A.; Mohan, R.; Annadurai, G.; Ahamed, M. In vitro antidiabetic and anti-inflammatory effects of Fe-doped CuO-rice husk silica (Fe-CuO-SiO2) nanocomposites and their enhanced innate immunity in zebrafish. *J. King Saud Univ. Sci.* **2022**, *34*, 102121. [CrossRef]
66. Vinotha, V.; Iswarya, A.; Thaya, R.; Govindarajan, M.; Alharbi, N.S.; Kadaikunnan, S.; Khaled, J.M.; Al-Anbr, M.N.; Vaseeharan, B. Synthesis of ZnO nanoparticles using insulin-rich leaf extract: Anti-diabetic, antibiofilm and anti-oxidant properties. *J. Photochem. Photobiol. B Biol.* **2019**, *197*, 111541. [CrossRef]
67. Rehana, D.; Mahendiran, D.; Kumar, R.S.; Rahiman, A.K. In vitro antioxidant and antidiabetic activities of zinc oxide nanoparticles synthesized using different plant extracts. *Bioprocess Biosyst. Eng.* **2017**, *40*, 943–957. [CrossRef]
68. Alkaladi, A.; Abdelazim, A.; Afifi, M. Antidiabetic Activity of Zinc Oxide and Silver Nanoparticles on Streptozotocin-Induced Diabetic Rats. *Int. J. Mol. Sci.* **2014**, *15*, 2015–2023. [CrossRef]
69. Dhobale, S.; Thite, T.; Laware, S.L.; Rode, C.V.; Koppikar, S.J.; Ghanekar, R.-K.; Kale, S.N. Zinc oxide nanoparticles as novel alpha-amylase inhibitors. *J. Appl. Phys.* **2008**, *104*, 094907. [CrossRef]

70. Kitture, R.; Ghosh, S.; More, P.A.; Date, K.; Gaware, S.; Datar, S.; Chopade, B.A.; Kale, S.N. Curcumin-Loaded, Self-Assembled Aloevera Template for Superior Antioxidant Activity and Trans-Membrane Drug Release. *J. Nanosci. Nanotechnol.* **2015**, *15*, 4039–4045. [CrossRef]
71. Dappula, S.S.; Kandrakonda, Y.R.; Shaik, J.B.; Mothukuru, S.L.; Lebaka, V.R.; Mannarapu, M.; Amooru, G.D. Biosynthesis of zinc oxide nanoparticles using aqueous extract of Andrographis alata: Characterization, optimization and assessment of their antibacterial, antioxidant, antidiabetic and anti-Alzheimer's properties. *J. Mol. Struct.* **2023**, *1273*, 134264. [CrossRef]
72. Sanap, S.P.; Ghosh, S.; Jabgunde, A.M.; Pinjari, R.V.; Gejji, S.P.; Singh, S.; Chopade, B.A.; Dhavale, D.D. Synthesis, computational study and glycosidase inhibitory activity of polyhydroxylated conidine alkaloids—A bicyclic iminosugar. *Org. Biomol. Chem.* **2010**, *8*, 3307–3315. [CrossRef] [PubMed]
73. Lawande, P.P.; Sontakke, V.A.; Kumbhar, N.M.; Bhagwat, T.R.; Ghosh, S.; Shinde, V.S. Polyhydroxylated azetidine iminosugars: Synthesis, glycosidase inhibitory activity and molecular docking studies. *Bioorganic Med. Chem. Lett.* **2017**, *27*, 5291–5295. [CrossRef] [PubMed]